Numerical modeling of seepage-induced liquefaction and slope failure

S.A. Bastani
Leighton Consulting, Inc., Irvine, California, USA

B.L. Kutter
University of California, Davis, California, USA

ABSTRACT: Several earth dams, tailings dams, and slopes failed or were severely damaged due to liquefaction during or after earthquakes. In seismic areas, earth structures such as embankments may be subjected to two forces: the static loads due to gravity and the inertia forces caused by earthquakes. In a significant number of cases, liquefaction-induced failure of embankments occurred from seconds to hours after an earthquake. In these cases, liquefaction reduced the material strength and the failure occurred only under static loads. A finite slope was modeled at UC Davis National Geotechnical Centrifuge to evaluate post-earthquake deformations with an injection-induced liquefaction system. A constitutive model was developed to capture the behavior of sands with a minimum number of physically meaningful parameters to enable prediction of post-earthquake liquefaction and/or seepage-induced liquefaction. This constitutive model is based on the Mohr-Coulomb constitutive model and the Critical State concept by adding three parameters to the conventional Mohr-Coulomb model. The constitutive model performed adequately for modeling the sand behavior under monotonic drained and undrained triaxial loading and water injection for a simple shear test under a constant shear stress. Using the new constitutive model, the failure mode of the centrifuge model due to seepage-induced liquefaction was studied utilizing *FLAC*. Stress and strain paths for specific elements in the embankment are studied and presented in this paper.

1 INTRODUCTION

Examples of post-earthquake liquefaction-induced failures of embankments are reported by Dobry & Alvarez (1967), Seed et al. (1975), Okusa et al. (1978), and Finn (1980). In these cases, liquefaction reduced the material strength and the failure occurred under static forces after the earthquake shaking. One mechanism for the delayed failure is the softening associated with redistribution of void ratio caused by gradients of pore water pressure in sloping ground with non-uniform permeability. This mechanism has been studied by Malvick et al. (2003) and Kokusho & Kojima (2002).

For the present study, the post-earthquake liquefaction-induced failure of granular embankments was investigated by a static centrifuge test in which the water that might be produced during an earthquake due to densification of deep saturated soil was simulated by injecting a similar volume of water at the base of the model as presented in detail by Bastani (2003). This centrifuge model consisted of a coarse sand layer with a constant thickness at its base to spread the injected water beneath an embankment composed of a fine sand capped by a layer of low permeability clayey silt.

The centrifuge test was modeled by Fast Lagrangian Analysis of Continua (*FLAC*) computer code utilizing a new constitutive model as presented in this paper. For more details on the centrifuge and numerical models refer to Bastani (2003).

2 CENTRIFUGE MODEL

The centrifuge model consisted of three layers:

1. A uniform 51 mm thick layer of Monterey Sand (mean grain size = 1.25 mm);
2. A fine sand (Nevada Sand, mean grain size = 0.12 mm) embankment with a minimum thickness of 102 mm at its toe and a maximum thickness of 356 mm at the slope crest; and
3. A uniform 51 mm thick layer of Yolo Loam that capped the Nevada Sand embankment.

The horizontal lengths of the embankment toe, the slope, and the crest were 356, 584, and 533 mm, respectively. The slope angle was 23.5 degrees. The average void ratio of the Nevada Sand was 0.77 corresponding to a relative density of 33 percent; at this density, the sand was highly dilative at the confining pressures experienced in the experiment. The Yolo Loam had an average undrained shear strength of

about 10 kPa and a water content of 33 percent. An additional overburden pressure equivalent to 90 mm of water head was applied over a plastic membrane on the Yolo Loam layer. All dimensions are provided in the model scale and the embankment's configuration is presented in Figure 1. The centrifuge model was consolidated in several stages as the centrifuge speed was increased up to 37.9 g.

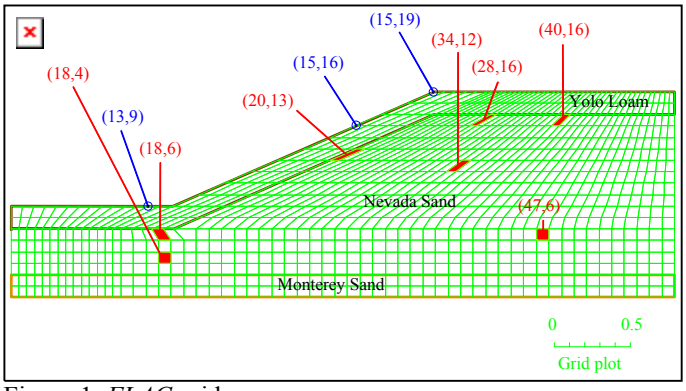

Figure 1. *FLAC* grid.

3 CONSTITUTIVE MODEL

A constitutive model was developed to simulate behavior of Nevada Sand in the *FLAC* program framework, and it was incorporated in the numerical modeling of the centrifuge test. The purpose of this model was to predict the principal behavior of Nevada Sand with a minimum number of parameters that are physically defined and measurable.

The failure envelope for this constitutive model corresponds to the Mohr-Coulomb constitutive model (shear yield function) with tension cutoff (tensile yield function). The shear flow rule is non-associated and the tensile flow rule is associated. The shear potential function corresponds to a non-associated flow rule. Details of Mohr-Coulomb model implementation are explained in the *FLAC* manual published by Itasca (2001).

Several modifications are made to the Mohr-Coulomb model. The mobilized friction angle ($\phi_{mobilized} = \phi_{cs} + \phi_{dilation}$) is represented as a sum of the critical state friction angle (ϕ_{cs}) and the dilation angle ($\phi_{dilation}$) as described by Bolton (1991). ϕ_{cs} is considered constant, while, the $\phi_{dilation}$ is assumed to be variable depending on the distance of the material state from the critical state line in e-log(p′) space, defined by the state parameter:

$$\psi = e - e_{cs} = e - (e_{cs})_a + \lambda \log \frac{p'}{p_a} \tag{1}$$

where e is the void ratio, $(e_{cs})_a$ is the critical state void ratio at one atmosphere, λ is the virgin compression slope, p' is the mean effective stress, and p_a is the atmospheric pressure.

As explained by Been & Jefferies (1985), the gradual change from dilative to contractive behavior can be quantified in terms of the state parameter ψ. The dilation angle ($\phi_{dilation}$) was modified based on the state parameter ψ and its changes according to the equation:

$$\phi_{dilation} = (\phi_{dilation})_0 \cdot (1 - \frac{\Delta\psi}{\psi}) \tag{2}$$

where $\phi_{dilation}$ is the updated dilation angle, $(\phi_{dilation})_0$ is the initial dilation angle, ψ is the state parameter, and $\Delta\psi$ is the variation of the state parameter. The soil's bulk and shear moduli are also modified in the model. The bulk modulus (K) is evaluated using the relation:

$$K = \frac{p'(1+e)}{\kappa} \tag{3}$$

where κ is the unloading slope and p' and e are defined as above. The shear modulus (G) was consequently determined based on the bulk modulus (K) and their elastic relationship:

$$G = \frac{3(1-2\upsilon)K}{2(1+\upsilon)} \tag{4}$$

where ν is Poisson's ratio.

The behavior of the constitutive model under selected load paths are presented in Figure 2: conventional drained triaxial compression, conventional undrained triaxial compression, and a simple shear element subjected to a constant applied shear stress and water injection. Results are shown for deviator stress (q), p', volumetric strain (ε_v), void ratio (e), and shear strain (γ).

This constitutive model predicted the strain hardening behavior of the Nevada Sand during undrained shearing until cavitation occurred prior to reaching the critical state line. The undrained path in Figure 2 approximately simulated the triaxial test data. Bastani (2003) compared the calculated undrained stress paths with experimental data (not shown here). The model behaved more stiffly under the undrained condition, approximately 2 times more than what was observed in the triaxial experiments for the Nevada Sand with a relative density of 26%; but the model reasonably matched test results for the Nevada Sand with a relative density of 39.4%.

The model behavior exhibited elastic contraction under the drained condition up to the peak shear stress. Dilation started after the peak shear stress and continued up to the critical state condition. Finally, the model behavior was studied under a constant shear stress and pore water pressure increase, modeling a simple shear test with pore fluid injection. The constitutive model slightly dilated prior to reaching the failure envelope; thereafter, the sample dilated with the increase of pore water pressure and the

stress path approached the origin along the failure envelope in the p'-q space until it reached the critical state condition similar to the stress path suggested by Boulanger (1990). The dilation rate was less than that shown by his experiment (Boulanger, 1990); however, the stress path, boundary condition, and initial condition of the experiments performed by Boulanger prior to water injection into his simple shear tests were not known, and therefore were not completely simulated by this calibration. As expected, the water injection to the element led to an unstable condition when the strength of the element dropped below the applied shear stress. Continued softening caused the stress path to drop toward the origin while the sample collapsed dynamically under the unbalanced external loads. Some oscillation is observed in the q-γ curves at shear strains greater than 0.12, but the softening behavior can still be clearly observed during the dynamic collapse.

The parameters used for this calibration and later in the numerical modeling based on this constitutive model are provided in Table 1.

Table 1. Model parameters.

Parameters	Value
λ*	0.022
κ (=λ/5)	0.0044
ϕ_{cs} (degree)	32
$(\phi_{dilation})_{max}$ (degree)	10
ν	0.25
e_o (initial void ratio)	0.77
$(e_{cs})_a$*	0.809
Atmospheric pressure, p_a (kPa)	101.2

* Archilleas et al. 2001.

4 *FLAC* MODEL BEHAVIOR

FLAC version 4.0 was utilized to model the centrifuge test. The numerical model was run twice. The first run used the conventional Mohr-Coulomb constitutive model, while the second run utilized the new constitutive model (discussed in Section 3) to model the Nevada Sand behavior. This numerical model was bounded with its and the constitutive model's limitations; however, it was successfully used to observe the general mechanism of localized increase in void ratio just beneath the less permeable clayey silt layer, and the failure mechanism; exact predictions were not expected. The *FLAC* runs were performed with the large-strain mode.

Figure 1 shows the grid utilized in this model. The grid nodes and elements are identified in the subsequent figures with their column and row numbers (i,j). The column and row numbers increase from left to right and bottom to top, respectively.

Contours of mobilized friction angle, volumetric strain, and shear strain and grid deformation patterns for the two runs are plotted on Figure 3. This figure indicates the following behaviors:

1. The mobilized friction angle was reduced along the Nevada Sand interface elements by the new constitutive model and along a deeper seated failure plane as shown by the new constitutive model;
2. Volumetric strains were concentrated along the interface of Nevada Sand and Yolo Loam in both numerical models. However, deeper volumetric strains were observed in the modified constitutive model, which coincided with the friction angle and shear strain patterns;
3. Shear strains were also concentrated at the slope interface within the Nevada Sand layer. Similarly a deeper shear zone was predicted by the new constitutive model matching the volumetric strain and mobilized friction angle reduction patterns;
4. Sand and clay layers moved downward at the slope, which was translated to vertical uplift at the toe.

It is worthwhile to mention that the pore water pressure was mainly increased from the slope toe within the Nevada Sand layer toward the slope crest and with a slower rate from the back of the slope crest toward the slope.

It should also be noted that the development of a deep failure mechanism, or not, was affected by the rate at which the water was injected relative to the permeability of the soils. For somewhat slower injection, the deeper mechanism would disappear and sliding along the bottom interface of the Yolo Loam would be apparent. For much greater injection rates, a failure mechanism at the interface between the coarse Monterey Sand and the fine Nevada Sand was observed (Bastani 2003).

Stress/strain paths of several elements at the toe, along the slope, and at the slope crest are plotted on Figure 4. Effective stresses of slope/leaning elements reduced while oscillating around constant shear stresses up to the failure envelope. However, shear stresses of carrying elements along the slope and its toe increased during the failure of leaning elements until reaching the failure envelope. Stress paths moved toward the origin after reaching the failure envelope and strain softening was observed. In general, the elements at the toe and along the slope showed higher shear strengths prior to their stress paths diving toward the origin in the second run due to the ability of the modified constitutive model to withstand a mobilized friction angle greater than the critical state friction angle during dilation. The majority of volumetric strains of elements were induced when the mean effective stress (p') became less than 10 kPa and close to zero. The volumetric strains were stabilized wherever the injection did not cause the strength to fall below the applied shear stress.

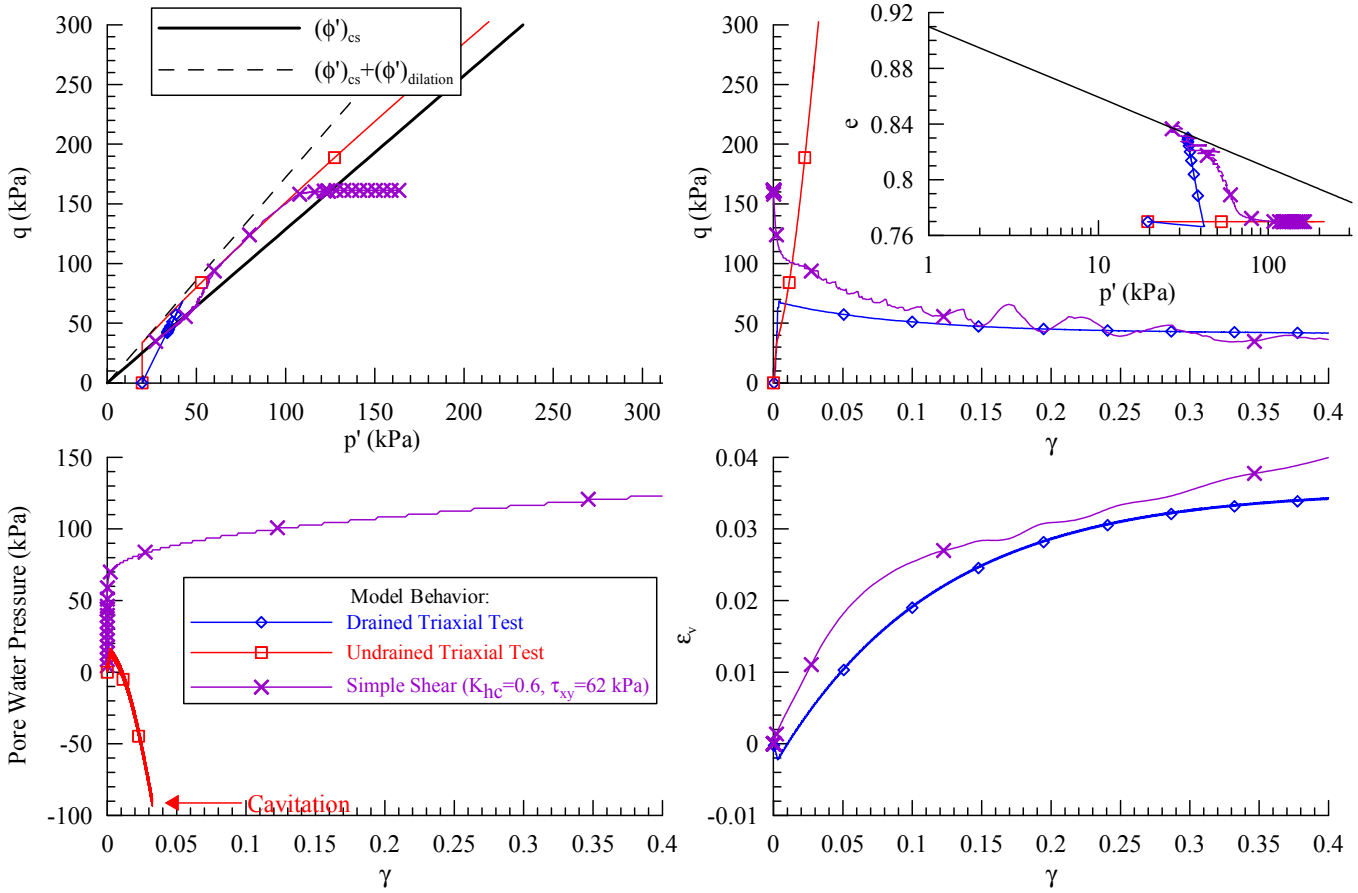

Figure 2. Behavior of the new constitutive model.

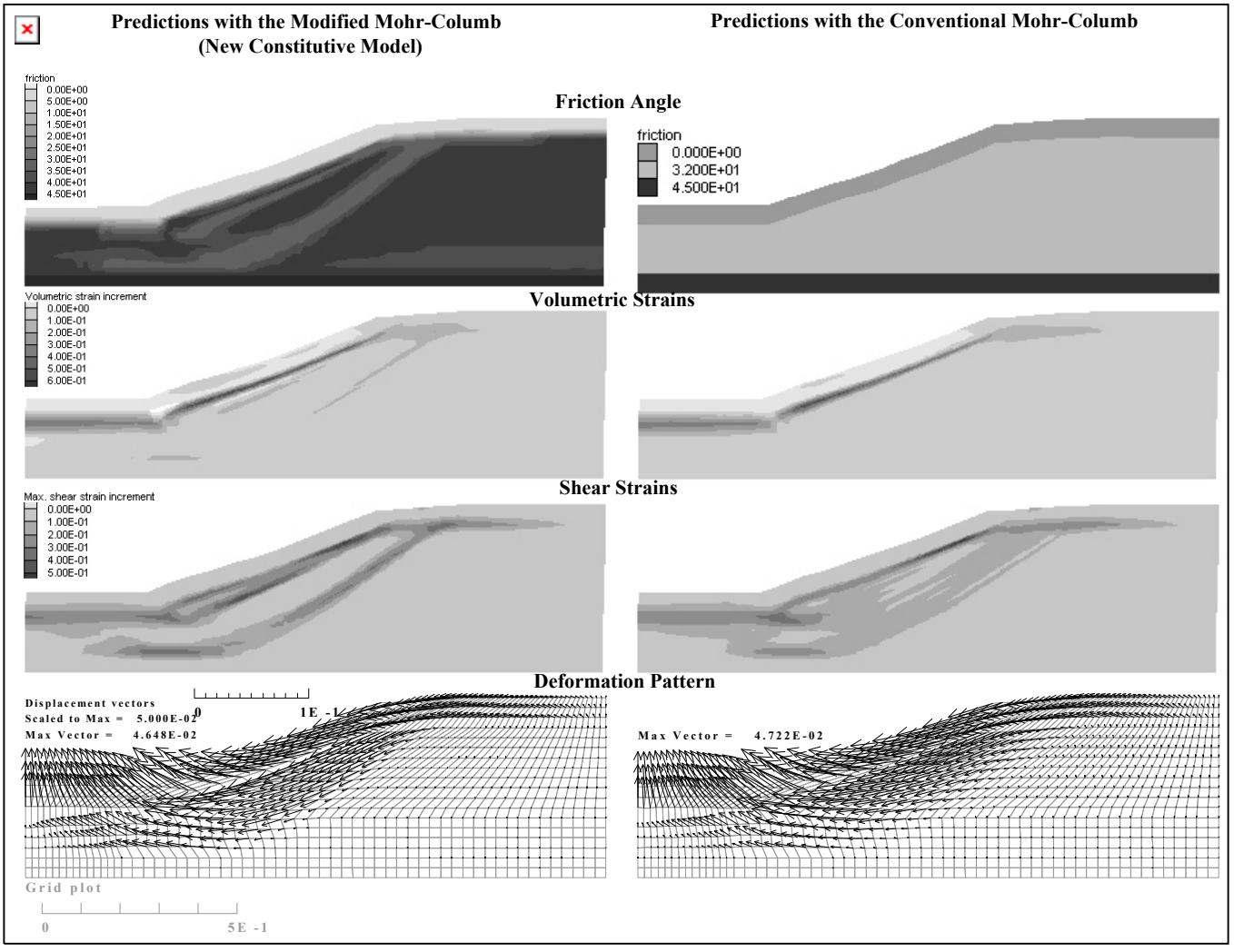

Figure 3. Friction angle, volumetric and shear strains, and deformation patterns at 13 seconds of seepage.

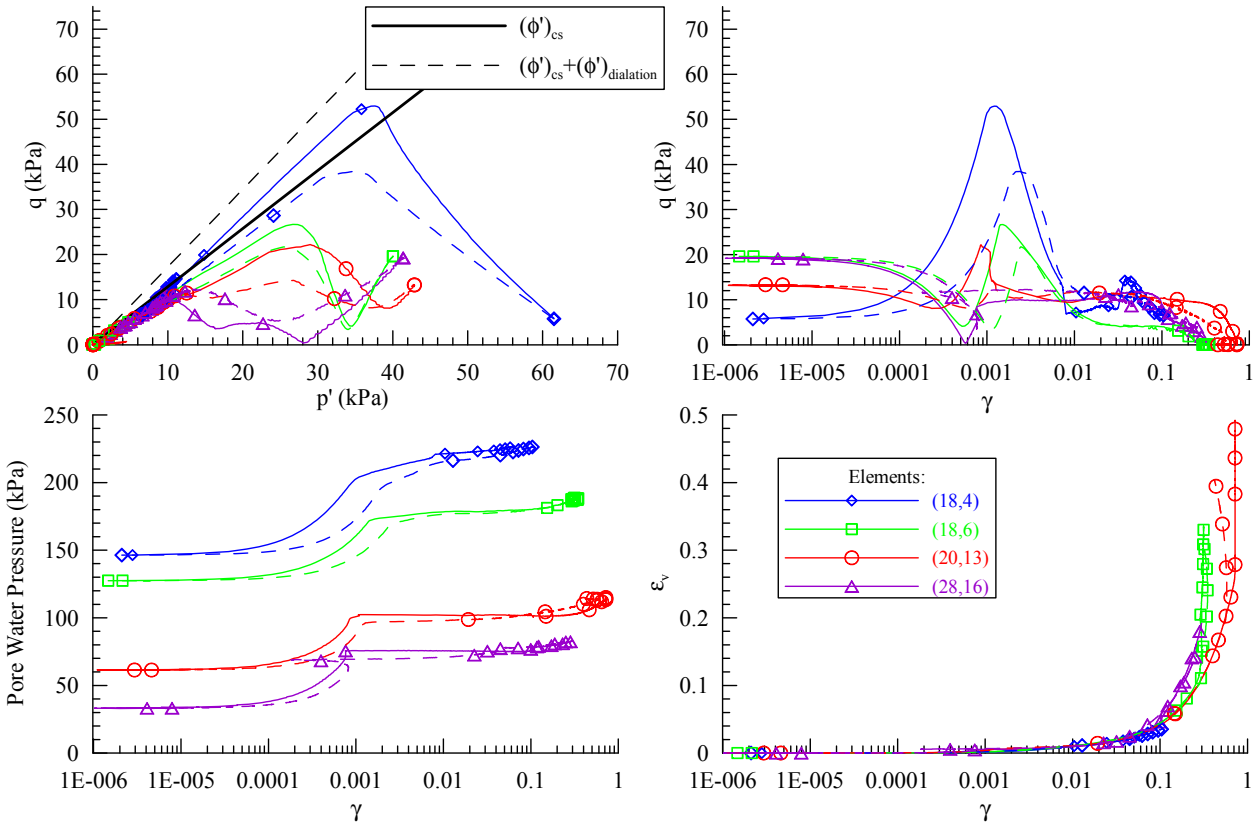

Figure 4. Stress path and behavior of elements. Solid and dashed lines refer to the results of the new and Mohr-Coulomb constitutive models, respectively.

Predicted pore water pressures and deformations are compared with the experimental results in Figures 5 & 6, respectively. In general the predicted pore water pressures are in good agreement with the experimental results for both constitutive models. However, the initial rate of pore water pressure increase is in better agreement with the new constitutive model. Similar trends were obtained by the numerical model, such as stabilization of pore water pressure at the beginning and its further increase for PPT# 5296 (Fig. 5). Other than deformation at the middle of the slope (LVDT #3), where the experimental result indicated bulging, deformation rates and magnitudes were predicted very well by both models.

The numerical model successfully predicted the dilatancy to cause a very loose layer of sand below the less permeable layer of Yolo Loam. The calculated volumetric strains of the dilated sand indicate a negligible residual strength after dilation.

5 CONCLUSION

A modified Mohr-Coulomb constitutive model was developed based upon critical state theory in conjunction with a new expression for dilatancy that depends on the state parameter (the distance between the state and the critical state). The constitutive model was shown to enable calculation of strain-softening paths, and dilation due to water injection.

The constitutive model was implemented in *FLAC* and used to analyze results of centrifuge model tests of layered sloping ground subject to pore fluid injection. The injection was intended to simulate the upward flow of water that might be generated by densification of deep soil deposits during earthquake shaking.

In the past, embankments made of dilative material were considered to be safe, because the undrained strength is greater than the driving stress (Poulos et al. 1985). The centrifuge tests and the *FLAC* analyses presented here clearly demonstrate the possibility that layers that impede drainage may cause a significant localized zone of softened material that should be considered a possibility in seismic design. To determine induced deformations due to local drainage of a system, a material model that captures this process should be incorporated in the numerical model. The mode of failure and local drainage of the centrifuge test presented here was successfully predicted utilizing the modified Mohr-Coulomb constitutive model in conjunction with *FLAC* numerical framework.

ACKNOWLEDGEMENT

The authors would like to thank Dr. Ben Hushmand, James Ward, and Vivian Cheng for reviewing this paper and providing constructive comments.

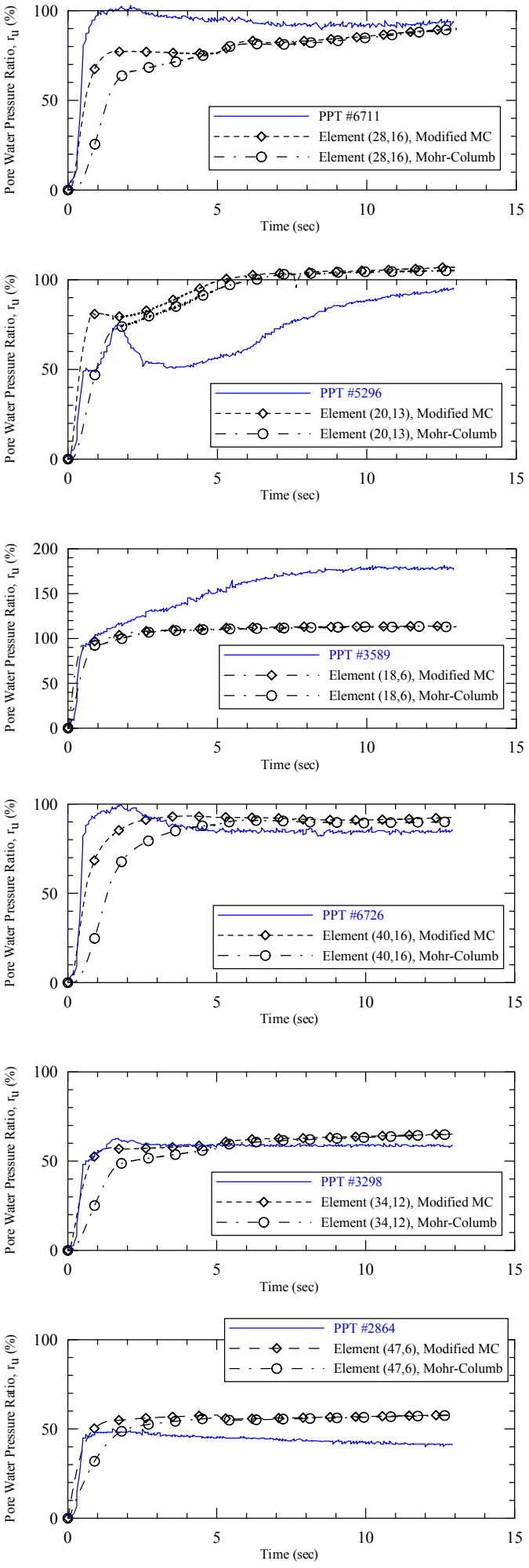

Figure 5. Pore water pressure time histories.

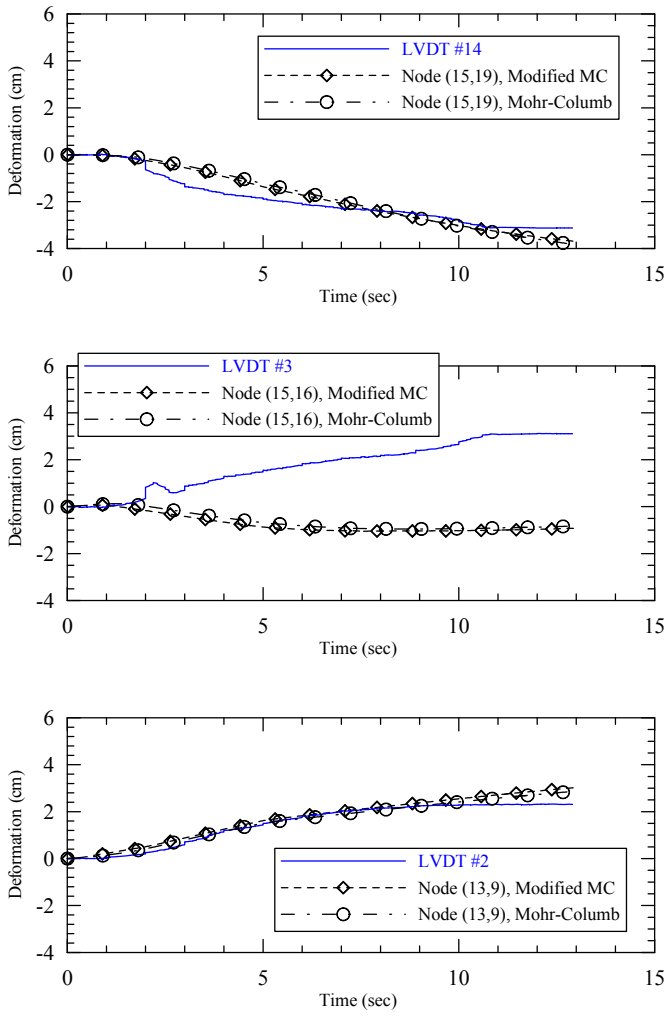

Figure 6. Deformation time histories.

REFERENCES

Archilleas, G.P., Bouckovalas, G.D., & Dafalias, Y.F. 2001. Plasticity Model for Sand Under Small and Large Cyclic Strains. *Journal of Geotechnical Engineering, ASCE* 127(11):.973-983.

Bastani, S.A. 2003. *Evaluation of Deformations of Earth Structures due to Earthquakes*. Dissertation presented to University of California, at Davis, in partial fulfillment of the requirements for the degree of Doctor of Philosophy.

Been, K. & Jefferies, M.G. 1985. A State Parameter for Sands. *Geotechnique* 35(2): 99-112.

Bolton, M. 1991. *A Guide to Soil Mechanics*. Published by M D & K Bolton, Printed by Chung Hwa Book Company, pp. 63-92.

Boulanger, R.W. 1990. *Liquefaction Behavior of Saturated Cohesionless Soils Subjected to Uni-Directional and Bi-Directional Static and Cyclic Simple Shear Stresses*. Dissertation presented to University of California, at Berkeley, in partial fulfillment of the requirements for the degree of Doctor of Philosophy.

Castro & Poulos (ASCE paper circa 1984).

Dobry, R. & Alvarez, L. 1967. Seismic Failure of Chilean Tailing Dams. *Journal of Soil Mechanics and Foundations Divisio*n, *Proceeding of the American Society of Civil Engineers* 93(SM6): 237-260.

Finn, W. D. 1980. Seismic Response of Tailing Dams. Presented at *Seminar on Design and Construction of Tailing Dams, Colorado School of Mines, Denver, Colorado*, pp. 76-97.

Itasca Consulting Group, Inc. 2001. *FLAC - Fast Lagrangian Analysis of Continua, Ver. 4.0 User's Manual*. Minneapolis, MN: Itasca.

Kokusko, T. & Kojima, T. 2002. Mechanism for Postliquefaction Water Film Generation in Layered Sand. *Journal of Geotechnical Engineering, ASCE* 128(2): 129-137.

Malvick, E.J., Kulasingam, R., Boulanger, R.W., & Kutter, B.L. 2003. Analysis of a Void Ratio Redistribution Mechanism in Liquefied Soil. To be Published in *Proceedings of the June 2003 Soil and Rock America Conference*.

Okusa, S., Anma, S., & Maikuma, H. 1978. Liquefaction of Mine Tailing in the 1978 Izu-Ohshima-Kihkai Earthquake, Central Japan. *Engineering Geology* Vol. 16, pp. 195-224, Elsevier Scientific Publishing Co.

Poulos, S.J., Castro, G., & France, J.W. 1985. Liquefaction Evaluation Procedure. *Journal of the Geotechnical Engineering Division, ASCE* 111(6): 772-792.

Seed, H.B., Lee, K.L., Idriss, I.M., & Makdisi, F.I. 1975. The Slides in the San Fernando Dams during the Earthquake of February 9, 1971. *Journal of the Geotechnical Engineering Division, ASCE* 101(GT7): 651.